JACS
JOURNAL OF THE AMERICAN CHEMICAL SOCIETY
Article
pubs.acs.org/JACS

Synthesis of Uniform Disk-Shaped Copper Telluride Nanocrystals and Cation Exchange to Cadmium Telluride Quantum Disks with Stable Red Emission

Hongbo Li,[†] Rosaria Brescia,[†] Mauro Povia,[†] Mirko Prato,[†] Giovanni Bertoni,[†,‡] Liberato Manna,[†] and Iwan Moreels*,[†]

[†]Istituto Italiano di Tecnologia, via Morego 30, IT-16163 Genova, Italy
[‡]IMEM-CNR, Parco Area delle Scienze 37/A, IT-43124 Parma, Italy

Supporting Information

ABSTRACT: We present the synthesis of novel disk-shaped hexagonal Cu_2Te nanocrystals with a well-defined stoichiometric composition and tunable diameter and thickness. Subsequent cation exchange of Cu to Cd at high temperature (180 °C) results in highly fluorescent CdTe nanocrystals, with less than 1 mol % of residual Cu remaining in the lattice. The procedure preserves the overall disk shape, but is accompanied by a substantial reconstruction of the anion sublattice, resulting in a reorientation of the *c*-axis from the surface normal in Cu_2Te into the disk plane in CdTe nanodisks. The synthesized CdTe nanodisks show a continuously tunable photoluminescence (PL) peak position, scaling with the thickness of the disks. The PL lifetime further confirms that the CdTe PL arises from band-edge exciton recombination; that is, no Cu-related emission is observed. On average, the recombination rate is about 25−45% faster with respect to their spherical quantum dots counterparts, opening up the possibility to enhance the emission rate at a given wavelength by controlling the nanocrystal shape. Finally, with a PL quantum efficiency of up to 36% and an enhanced PL stability under ambient conditions due to a monolayer of CdS formed on the nanocrystal surface during cation exchange, these flat quantum disks form an interesting enrichment to the current family of highly fluorescent, shape-controlled nanocrystals.

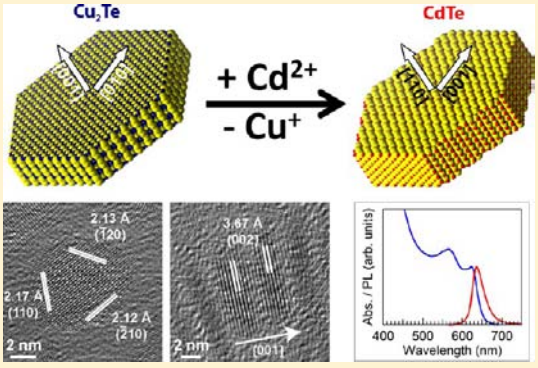

INTRODUCTION

In recent years, we have seen remarkable progress in the size- and shape-control of colloidal nanocrystals. Next to spherical core and core/shell quantum dots,[1,2] the synthesis of nanowires and nanorods is already well established,[3−5] and by now several protocols also allow extending their shape to flat nanodisks and larger 2D nanosheets.[6,7] Recent developments have also produced flat core/shell nanocrystals, for example, CdSe/CdS nanocrystals with a dot-in-disk motive yielding an emission strongly polarized in two dimensions,[8] or 2D CdSe nanosheets passivated with a thin layer of CdS via solution atomic layer deposition.[9]

Compared to the synthesis of quantum dots and rods, for several materials it is still challenging to prepare fluorescent quantum disks, that is, 0D quantum confined flat or highly oblate nanocrystals. Indeed, while this shape is easily obtained in copper sulfide and selenide nanocrystals,[10−12] for II−VI, IV−VI, or other chalcogenide materials only larger 2D sheets are grown, by either exfoliation of thin films or oriented attachment of small clusters, in both cases leaving little control over the lateral dimensions.[6,13−15] Yet from both a structural and optical perspective, nanodisks may show advantages over extended sheets: we can expect an improved control over their assembly into superlattices,[16] and a continuous tunability of their band-edge absorption and photoluminescence (PL) by varying the dimensions of the disk. To this end, the control over all spatial dimensions of the nanodisk is of course crucial.[13,17]

For nanocrystal compositions and shapes that are difficult to grow by direct synthesis approaches, cation exchange reactions have emerged as an extremely useful alternative route.[18−20] Recently, copper chalcogenides were recognized as a high quality template for cation exchange.[21,22] Furthermore, as in this material class several disk-shaped nanocrystals are already reported in literature,[10,23] we can take full advantage of both features. In this paper, we first present the synthesis of novel Cu_2Te nanodisks with controlled thickness and diameter, as protocols are far less developed compared to copper sulfide and selenide nanocrystals.[24−26] Next, we perform a cation exchange reaction to obtain highly fluorescent CdTe quantum disks, paying particular attention to the preservation of the overall shape. As a result of the hexagonal crystal structure of the initial Cu_2Te disks, we obtained wurtzite CdTe quantum disks. This is a metastable phase at room temperature for bulk CdTe, and

Received: May 10, 2013
Published: July 18, 2013

   dx.doi.org/10.1021/ja404694k | J. Am. Chem. Soc. 2013, 135, 12270−12278

therefore, the resulting optoelectronic properties of the quantum disks may be of particular interest. The passivation of the surface with sulfur atoms, due to the thiol ligands used in the copper telluride synthesis, and the conservation of this layer in the following cation exchange reaction leads to an enhanced PL stability of the CdTe quantum disks compared to spherical CdTe quantum dots prepared by a conventional approach. The PL quantum efficiency was as high as 36%, and we observed a faster PL decay rate compared to the quantum dots, which we could attribute (in part) to a reduced average dielectric screening induced by the peculiar shape of the disks.

EXPERIMENTAL SECTION

Materials. Cadmium oxide (CdO, 99.999%), trioctylphosphine (TOP, 97%), and elemental tellurium (Te, 99.99%) were purchased from Strem Chemicals. Copper(II) acetylacetonate ($Cu(C_5H_7O_2)_2$, 99.99%), octylamine (99%), oleylamine (70%), oleic acid (90%), 1-octadecene (90%), 1-octanethiol (C_8SH, 98.5%), 1-dodecanethiol ($C_{12}SH$, 98%), 1-octadecanethiol ($C_{18}SH$, 98%), anhydrous ethanol, and toluene were purchased from Sigma-Aldrich. All chemicals were used without further purification.

Synthesis of Copper Telluride Nanodisks. Copper telluride nanodisks were prepared by modification of a routine reported for the synthesis of spherical nanocrystals.[24] In detail, a trioctylphosphine-Te solution (TOPTe, typically 10 wt % Te in TOP, i.e., molar TOP/Te ratio of 3:1) was prepared first, by dissolving Te powder in TOP at 250 °C under nitrogen for 3 h, until the Te completely dissolved. The TOPTe solution was subsequently cooled to room temperature before use in the synthesis. In another flask, a mixture of 1.0 mmol of copper acetylacetonate (262 mg), 5 mL of $C_{12}SH$, and 10 mL of oleic acid was heated to 100 °C and kept for 60 min under vacuum to prepare the copper precursor. Hereafter, the temperature was raised to 180 °C to form a clear solution. Once the temperature stabilized, 640 mg of the 10 wt % TOPTe solution was quickly injected. The reaction was kept at 180 °C for 2 min and then cooled to 80 °C. At this temperature, 1 mL of octylamine and 2 mL toluene were added to improve the colloidal stability of the nanodisks and further quench the reaction. Purification of the nanodisks was performed by adding an excess of ethanol to precipitate them, followed by centrifugation and resuspension in toluene. This process was repeated to ensure complete removal of excess ligands and unreacted precursors. To control the nanodisk diameter and thickness, we varied the reaction time and temperature, precursor concentrations, and the thiol ligand length.

Cation Exchange Reaction to CdTe Quantum Disks. CdTe quantum disks were obtained by cation exchange reaction from copper telluride, according to previously reported approaches.[27,28] In order to perform the exchange, a Cd cation solution was prepared separately by dissolving 1 mmol of CdO powder in a mixture of 4 mmol of oleic acid and 4 mL of octadecene at 240 °C, until we obtained a transparent solution. Hereafter, the solution was cooled to 180 °C, and the copper telluride nanodisks dispersed in TOP were swiftly injected into the cadmium oleate solution (Cd/Cu molar ratio of 100:1). TOP is an important chemical in cation exchange reactions based on copper chalcogenides templates. As it is a soft base with a strong tendency to bind to copper ions, it can efficiently extract copper from the lattice.[18] The reaction proceeded for 5 min, during which we observed a change in color from the typical brown of copper telluride into dark red, indicating a successful exchange. After synthesis, the samples were purified by adding an excess of ethanol to precipitate the obtained CdTe quantum disks, and they were finally redispersed in toluene.

Structural Characterization and Elemental Analysis. X-ray diffraction patterns were collected with a Smartlab 9 kW Rigaku diffractometer equipped with a copper rotating anode. Samples were prepared by dropcasting of a nanocrystal suspension onto a Si(111) miscut substrate (7° toward the (110) plane). Bright-field transmission electron microscopy (BF-TEM) images and selected area electron diffraction (SAED) patterns were acquired using a 100 kV JEOL JEM-1011 microscope. For the determination of the nanodisks' diameter and thickness, typically 100−200 particles were measured. High-resolution TEM (HRTEM) images were obtained in a 200 kV ultrahigh-resolution microscope (JEOL JEM-2200FS) equipped with a field emission gun and a CEOS image aberration corrector. High angle annular dark field (HAADF) images, acquired in scanning TEM (STEM) mode, and energy dispersive X-ray spectroscopy (EDS) analyses were performed on the same instrument, with a Bruker Quantax 400 system with a 60 mm^2 XFlash 5060 silicon drift detector. For HRTEM analyses, nanocrystal dispersions were drop-cast onto copper grids covered with an ultrathin amorphous carbon film suspended onto a lacey carbon net, while for EDS analysis they were deposited onto carbon-coated aluminum grids and the measurements were carried out using a holder with a beryllium cup. HAADF-STEM (annular aperture of 46 mrad, probe size 1 nm) was used because of the dominating incoherent nature of its signal, permitting to identify the shape of the nanocrystals by the inspection of their profiles in the HAADF-STEM images. Simulations of the HAADF-STEM profiles were carried out using the software STEM-CELL.[29]

X-ray photoelectron (XPS) characterization was performed on a Kratos Axis Ultra DLD spectrometer, using a monochromatic Al Kα source (15 kV, 20 mA). Samples for XPS were prepared by drop casting 20 μL of a solution containing the nanodisks on a highly oriented pyrolytic graphite (HOPG) substrate. High resolution narrow scans were performed at a constant pass energy of 10 eV and steps of 0.1 eV. The photoelectrons were detected at a takeoff angle $\Phi = 0°$ with respect to the surface normal. The pressure in the analysis chamber was maintained below 7×10^{-9} Torr for data acquisition. The binding energy (BE) scale was internally referenced to the C 1s peak (BE for C−C = 284.8 eV). Inductively coupled plasma optical emission spectroscopy (ICP-OES) was performed on a Thermo Scientific iCAP 6500 spectrometer. Samples for the ICP analysis were prepared by digestion of the dried nanodisks with aqua regia for 12 h, followed by dilution with Milli-Q water.

Optical Spectroscopy. Absorption spectra were recorded with a Varian Cary 5000 UV−vis-NIR absorption spectrophotometer. The emission was collected using an Edinburgh Instruments FLS920 spectrofluorometer. Samples were dried and dispersed in chloroform, with an optical density of about 0.1 cm^{-1} at 500 nm. The PL quantum efficiency of the CdTe quantum disks was measured with an integrating sphere, exciting the samples at 500 nm. The lifetime was collected via time-correlated single-photon counting, exciting the sample at 400 nm with a 50 ps laser diode at a repetition rate of 1 MHz to ensure complete decay of the emission between the excitation pulses. The emission was measured at the peak position, with a typical emission bandwidth of 4 nm. For the spectral dependence, a bandwidth of 2 nm was used.

RESULTS AND DISCUSSION

Figure 1 shows typical TEM images of the copper telluride nanodisks. The average diameter and thickness are 10.1 and 2.3 nm, respectively, with a corresponding size dispersion (standard deviation) of 0.7 and 0.2 nm (histograms are shown in Figure 1c and d). Due to the narrow size distributions, we can observe spontaneously assembled face-to-face disks standing on their edge on the TEM grid. By adding a nonsolvent (acetonitrile) to the solution as described in our previous paper on the assembly of branched NCs,[30] we could even induce large-area formation of face-to-face nanoribbons and superlattices thereof, which confirms the size homogeneity throughout the sample (see Supporting Information, Figure S1).

The XPS characterization (Figure 2a−c) yields a Cu/Te stoichiometry of 2.2:1. This ratio is confirmed by ICP-OES measurements which yield 2.1:1, and indicates the formation of quasi-stoichiometric Cu_2Te, with a slight Cu excess probably located at the nanodisk surface. Additionally, the Auger parameter for Cu, calculated as the sum of the binding energy of Cu $2p_{3/2}$ peak (BE Cu $2p_{3/2}$ = 932.3 ± 0.1 eV, panel a) and

dx.doi.org/10.1021/ja404694k | J. Am. Chem. Soc. 2013, 135, 12270−12278

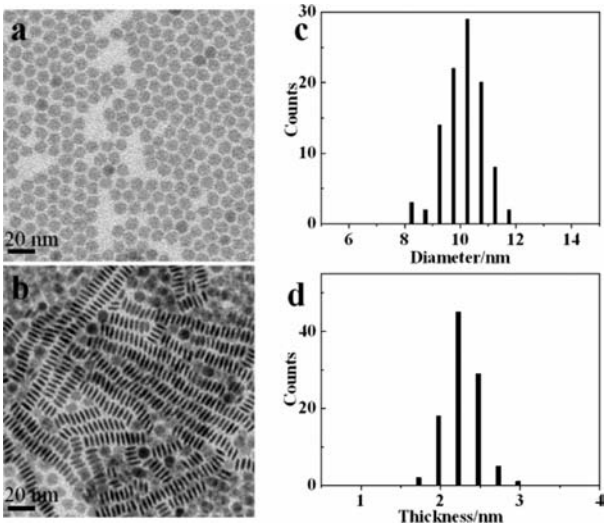

Figure 1. (a,b) BF-TEM images of copper telluride nanodisks. Nanodisk stacks allow determining their thickness. (c,d) Corresponding size histograms showing the diameter and thickness of the nanodisks. The histograms were constructed using a binning of 0.5 and 0.25 nm for the diameter and thickness, respectively.

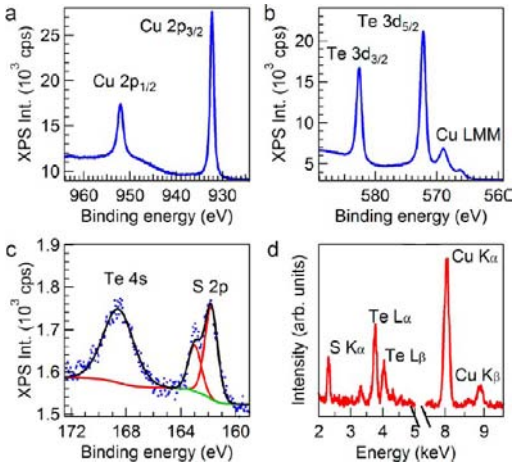

Figure 2. (a–c) XPS analysis on the copper telluride nanodisks: (a) Cu 2p doublet, (b) Te 3d doublet and Cu LMM Auger peak, and (c) Te 4s and S 2p peaks, together with data fitting for quantitative comparison. Shirley-type background and voigt profiles were used in the procedure. S 2p doublet separation was set to 1.2 eV. (d) EDS overview spectrum, obtained on an area containing several Cu_2Te nanodisks.

of the kinetic energy of the Cu LMM Auger peak (KE Cu LMM = 917.6 eV, panel b), is equal to 1849.9 eV, in agreement with data already reported for Cu(I) chalcogenides,[31] and no satellites typical of Cu(II) species are observed (Figure 2a). The positions of the Te $3d_{5/2}$ and Te $3d_{3/2}$ peaks, shown in panel b, are at 572.2 and 582.6 eV, respectively, in agreement with values reported for the (−2) oxidation state of Te.[27] Both results further support the formation of pure Cu_2Te, free from copper-deficient $Cu_{(2-x)}Te$, $0 < x \leq 1$. Moreover, since no Te $3d_{5/2}$ peaks are present around 576–577 eV, we can also exclude the presence of tellurium oxides (Te $3d_{5/2}$ BE for TeO_2: 575.9 ± 0.2 eV; Te $3d_{5/2}$ BE for TeO_3: 577 ± 0.3 eV).[32] In panel c, the XPS results collected on the Te 4s and S 2p peaks are reported. A quantitative analysis yields a S/Te ratio of 0.2:1, in line with the ratio obtained from EDS (0.3:1 in the sample shown in Figure 2d), and ICP-OES, where we found an average S/Te ratio of 0.24:1 by evaluation of seven Cu_2Te samples. Both results indicate the presence of $C_{12}SH$ ligands bound to the surface of the nanodisks.

XRD diffractograms recorded at room temperature on the Cu_2Te nanodisks did not yield a clear pattern (Supporting Information, Figure S2). Briefly annealing the sample at 100 °C in vacuum however significantly improved the result, as the sharp reflections, probably arising from organic impurities, were removed (Figure 3a). The remaining pattern corresponded to a

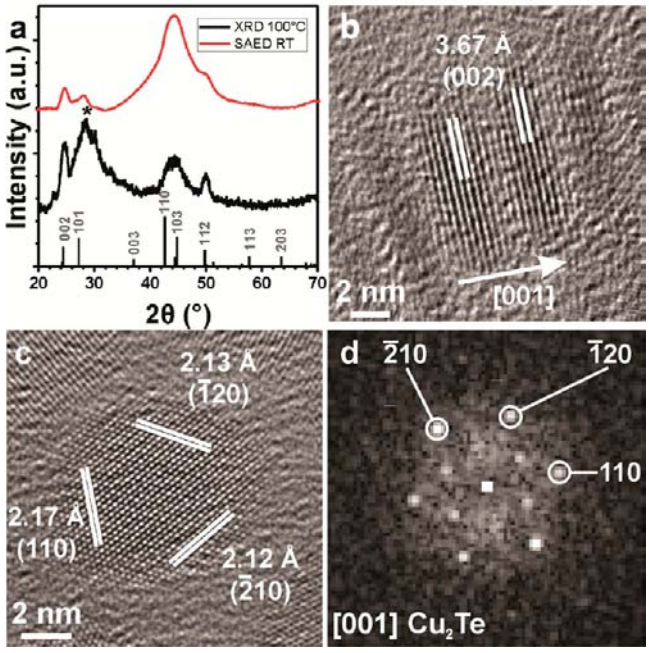

Figure 3. (a) XRD pattern collected on Cu_2Te nanodisks after a short annealing in vacuum at 100 °C, compared to the radially integrated intensity profile from a SAED pattern acquired at room temperature from a region including several Cu_2Te nanodisks. Both patterns exhibit a good match with hexagonal Cu_2Te (space group *P6/mmm*, ICSD structure #77055). The asterisk (∗) marks a broad reflection arising from the miscut silicon (111) substrate. (b–c) HRTEM images of (b) disk stacks, showing the [001] direction of Cu_2Te oriented perpendicular to the surface for each nanodisk, and (c) a disk with the flat face parallel to the support film. (d) The fast Fourier transform (FFT) of (c) shows the [001] pattern of Cu_2Te, confirming that the *c*-axis is perpendicular to the flat face of the disks. The HRTEM images were frequency-filtered, in order to emphasize the crystalline features.

Cu_2Te nanocrystal possessing a hexagonal crystal symmetry (*P6/mmm* space group, ICSD structure no. 77055). Results were confirmed by measuring the SAED pattern of a collection of Cu_2Te nanodisks at room temperature. The integrated signal again shows a good match with the same Cu_2Te crystal structure (Figure 3a). The SAED pattern is also in agreement with the (room-temperature) HRTEM measurements, which exhibit single-crystal nanodisks of the same phase (Figure 3b–d). The data further revealed that the [001] direction is oriented perpendicular to the plane of the Cu_2Te nanodisks, similar to the case of Cu_2S nanodisks reported by Sigman et al.[10]

The average thickness and diameter of as-synthesized Cu_2Te nanodisks can be tuned by changing the growth time and temperature, and the concentration of the TOPTe solution. In general, higher temperatures resulted in thicker nanodisks, yet

dx.doi.org/10.1021/ja404694k | J. Am. Chem. Soc. 2013, 135, 12270–12278

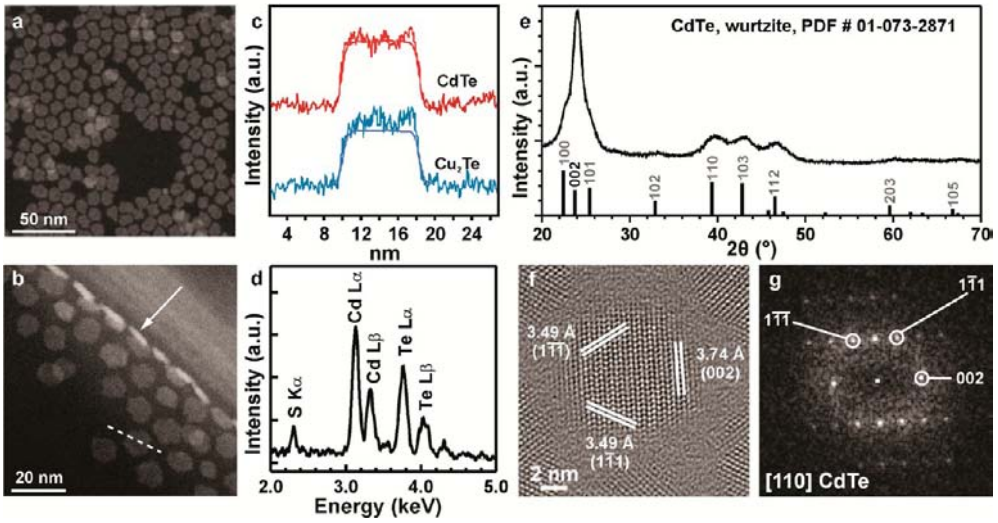

Figure 4. (a) HAADF-STEM overview image of the CdTe quantum disks. (b) Some disks (e.g., the one pointed by the arrow) adhere vertically to the lacey carbon net edge, allowing unambiguous determination of their shape. (c) Comparison of the HAADF-STEM intensity profiles (typically along the direction as indicated in (b) by the dashed line) from a CdTe quantum disk and a Cu_2Te nanodisk, together with their respective simulated profile, confirming the flat top and bottom surface of both systems. The simulation was convolved with a probe size of about 1 nm, to take into account the experimental resolution. (d) EDS spectrum acquired over several CdTe nanodisks, showing contributions from the Cd- and Te-core atoms, and S-atoms from the $C_{12}SH$ ligands. (e) XRD pattern, in agreement with wurtzite CdTe (space group *P*63*mc*, JCPDS card no. 01-0732871). (f) HRTEM image of a typical CdTe quantum disk and (g) corresponding FFT demonstrating that the flat surface is parallel to a [110]-oriented plane of wurtzite CdTe.

with a smaller diameter. For instance, Cu_2Te nanodisks with a thickness of 2.2 nm and a diameter of 12 nm were prepared at a temperature of 175 °C. By increasing it a mere 10 °C, the diameter was reduced to 8 nm and the thickness increased to 3.2 nm. Interestingly, a lower and higher limit for the temperature was observed at 160 and 200 °C, respectively, where in both cases spherical nanocrystals were obtained, with diameters of 4.6 nm (Supporting Information, Figure S3a) and 7.4 nm (Supporting Information, Figure S3b), respectively. Elemental analysis via ICP-OES yielded an elevated concentration of sulfur in the latter case (atomic ratio of S/Te equal to 1.2:1), due to the decomposition of $C_{12}SH$ at 200 °C. This is consistent with reported results that $C_{12}SH$ can be used as sulfur source to prepare monodisperse copper sulfide nanocrystals at a temperature of 230 °C.[33]

Reducing the Te concentration to 5 w % (thus injecting a larger amount of TOPTe to maintain a constant Cu/Te ratio) also suppressed the formation of nanodisks at 180 °C (Supporting Information, Figure S4). Higher concentrations of Te (i.e., 15 wt % TOPTe) on the other hand facilitated the formation of nanodisks with larger lateral dimensions (12 nm diameter vs 8 nm as described above). It is clear that the experimental conditions (temperature, ligand length, precursor concentrations) to obtain Cu_2Te nanodisks of uniform size and shape lie in a narrow range. Even when varying the thiol chain length using C_8SH, $C_{12}SH$, or $C_{18}SH$, we only observed the formation of nanodisks for $C_{12}SH$ (Supporting Information, Figure S5). Nevertheless, under the appropriate conditions, high quality Cu_2Te can be readily synthesized, with a typical diameter varying between 8 and 12 nm, and a thickness between ca. 2 and 3.5 nm (see Supporting Information Table S1 for a summary of synthesis conditions).

In agreement with earlier literature results on spherical and rodlike nanocrystals,[27,28,34] the Cu^+ cations could be exchanged to Cd^{2+} while maintaining the shape of the nanocrystals. Figure 4a,b shows HAADF-STEM images, including a side view of some CdTe nanodisks adhered to the walls of the lacey carbon net. The intensity profiles determined from the HAADF-STEM images (Figure 4c) also matched well with a simulated profile from an ideal nanodisk with flat surfaces.

Interestingly, in contrast with the typical Cd^{2+} to Cu^+ exchange reaction proceeding swiftly under ambient room temperature conditions,[35] here we needed to raise the temperature before a cation exchange was observed. Indeed, when adding a 30-fold excess of Cd-oleate to a solution of Cu_2Te nanodisks and keeping it for 24 h at 50 °C, the chemical composition (obtained via ICP-OES) did not show any substantial incorporation of Cd into the lattice (Table 1). At a temperature of 100 °C, a partial exchange was obtained after 60 min. A further increase of the temperature to 150 °C resulted in a nearly complete exchange in 5 min, with finally less than 1% of Cu typically remaining at 200 °C. Above this temperature, full exchange occurred, yet at the expense of a reshaping of the particles into spherical CdTe nanocrystals (Supporting Information, Figure S6).

Table 1. The Exchange Efficiency Was Evaluated by Performing the Cation Exchange Reactions at Different Temperatures, Followed by ICP-OES Analysis of the Chemical Composition of the Obtained Nanocrystals[a]

temp	reaction time	final Cd/Cu ratio
50 °C	24 h	4%
100 °C	1 h	52%
150 °C	5 min	97%
200 °C	5 min	99%

[a]For these reactions, we added a 30-fold excess of Cd-precursors, compared to the total amount of Cu atoms present. The reactions above 100 °C were stopped after 5 min.

Cation exchange reactions occurring at elevated temperatures have been observed in other systems. For instance, previously

dx.doi.org/10.1021/ja404694k | J. Am. Chem. Soc. 2013, 135, 12270−12278

we performed cation exchange reactions at 250 °C to completely remove residual copper ions from ZnSe/ZnS quantum rods, in order to obtain efficient band edge luminescence.[28,34] Beberwyck et al. reported the preparation of III–V InP and InAs nanocrystals via an ion exchange reaction from Cd_3P_2 and Cd_3As_2, respectively, wherein a temperature of 300 °C was necessary to induce the exchange in the strongly bound covalent lattice.[19] IV–VI PbX (X = S, Se, Te) nanocrystals can be passivated with an outer shell of CdX via cation exchange, yet also there the temperature needs to be raised over 100 °C before a reaction occurs, above which the shell thickness is mainly determined by the growth temperature.[36,37]

After the cation exchange reaction, we obtained crystalline CdTe nanodisks with a Cd/Te atomic ratio of 1.3:1 (measured with EDS, Figure 4d) and a wurtzite crystal structure (space group $P6_3mc$, JCPDS card no. 01-0732871, Figure 4e). However, the XRD pattern showed an especially narrow peak for the (002) reflection, suggesting that the *c*-axis now lies in the nanodisk plane. Note that a second narrow peak for the (004) reflection should be observed; however, the intensity of the (004) reflection in bulk wurtzite CdTe is only 0.1% compared to the highest intensity and hence this peak is not discernible in our XRD pattern. From the line width of the (002) reflection, the Scherrer equation $D = K\lambda/(\beta \cos \theta)$, with D being the crystallite size, λ the X-ray wavelength, β the full width at half-maximum of the diffraction peak, θ the Bragg angle, and $K = 0.9$, yields a crystallite coherence length of 8.1 nm along the [001] direction (see Supporting Information, Figure S10). Applying the Scherrer equation to the width of the (110) peak results in a 2.8 nm size along the [110] direction. The other XRD reflections yield sizes ranging from 2.8 to 3.3 nm, with slight variation due to the different directions probed. Data are in agreement with the TEM images, where we obtained an average diameter of 10 nm and a thickness of 2.9 nm. The peculiar orientation of the CdTe quantum disks was further confirmed by the measurement of the crystal structure on single disks using HRTEM (Figure 4f,g). The images give direct evidence that the [001] direction lies in the plane of the nanodisks.

In the present study, as the cation exchange is conducted on anisotropic nanocrystals, we are given a unique insight into the exchange mechanism. Knowing that the exchange occurs between hexagonal crystals with highly similar lattice constants (a_1 = 4.23A° and c_1 = 7.27A° for Cu_2Te, ICSD structure # 77055, and a_2 = 4.57A° and c_2 = 7.47A° for CdTe, JCPDS card no. 01-0732871) yet with different orientation of the *c*-axis (Figure 5a), we compared the underlying Te sublattice before and after exchange. Figure 5b,c clearly shows that the exchange can only occur when it is accompanied by slight displacements of the Te anions, to accomplish the evolution from Cu_2Te disks terminated by (001) basal planes to CdTe disks terminated by (110) basal planes. First, we note that in both structures the Te atoms form separate columns when viewed from the (flat) top; that is, there is no mixing with cations in the columns. Let us consider then the four Te atoms in the (001) plane in Cu_2Te (magenta atoms in Figure 5b,c). These Te anions shift position in CdTe, with two atoms staying on the new (110) plane, and two atoms moving down (or equivalently up) to form the second (110) plane in CdTe. The in-plane displacements are quite small (about 0.3 Å) resulting in a slight distortion of the projected hexagonal Te lattice (giving an in-plane projected area compressed by about 5%). The main displacements are

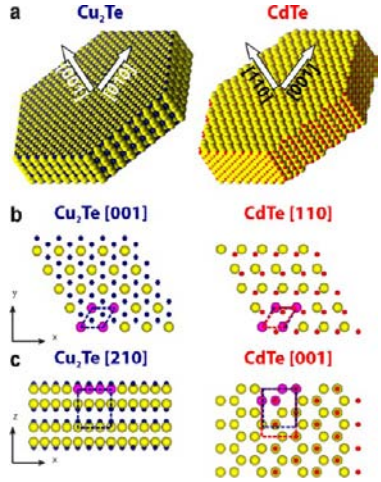

Figure 5. (a) Sketches of the Cu_2Te and CdTe disks, with arrows indicating the respective crystal orientations. (b,c) Schematic views of slabs of the Cu_2Te and CdTe structures, showing a few atomic layers of the nanodisks according to the respective phases and orientations determined by HRTEM. Each Te anion (larger yellow spheres) in the (001) plane of Cu_2Te forms a hexagonal lattice (cell indicated by blue dashed lines) with the three neighboring anions (magenta) on the same plane. The (110) anionic sublattice in wurtzite CdTe still resembles a distorted hexagon in projection (red dashed lines). However, the Te atoms of the original Cu_2Te structure have to move considerably in the *z*-direction to adapt the Cd atoms and form the two (110) layers in wurtzite CdTe. The volume occupied by the same number of Te atoms is included within the blue and red frames in Cu_2Te and CdTe, respectively.

along the *z* direction, resulting in a splitting of a pristine (001) Te-plane of Cu_2Te into the (110) Te "bilayer" of CdTe. Considering also the Te atoms from the layers underneath, the average displacement per Te atom along *z* is about 1.9 Å (given by the difference $2a_2 - c_1$).

This reconstruction effectively tilts the *c*-axis into the plane of the nanodisks, and additionally leads to an overall increase in thickness of about 25% after cation exchange. To verify this, we measured the thickness in a sample of Cu_2Te nanodisks, and the corresponding CdTe disks. We obtained (1.85 ± 0.09) nm and (2.26 ± 0.10) nm for the average thickness of Cu_2Te and CdTe, respectively, suggesting an increase in thickness of 22% (errors represent 95% confidence intervals). Two other samples yielded (2.30 ± 0.14) nm vs (2.11 ± 0.13) nm (8% decrease), and (2.38 ± 0.11) nm vs (2.92 ± 0.17) nm (23% increase), respectively. Hence, in agreement with the calculations, the TEM measurements suggest an increase in thickness of about 12%. The experimental observations and corresponding modeling show that changes are small enough to maintain the overall shape of the nanocrystal, yet they are likely sufficient to lead to the temperature-activation of the exchange reaction, as it implies that the exchange requires sufficient thermal energy for the atoms to hop to the new lattice sites. While a complete clarification of the driving force behind the reconstruction requires further total energy calculations, computational studies on bulk facets of wurtzite CdSe have already shown that most ligands have higher binding affinities for the nonpolar (100) and (110) facets in this material than for the (001) and (00−1) facets,[38,39] so that in general the nonpolar facets in surfactant-passivated NCs tend to have a lower surface energy and consequently a larger surface area than the polar ones. A similar situation should apply here, aided by the possibility for the

dx.doi.org/10.1021/ja404694k | J. Am. Chem. Soc. 2013, 135, 12270–12278

lattice to reorganize during cation exchange, under the constraint of overall preservation of the crystal shape. Such reorganization, favored by the high temperature at which the exchange is performed, appears to drive the system to a low-energy configuration characterized by CdTe nanodisks that are terminated by large (110) and (−110) top and bottom facets. Considering that cation exchange reactions often occur between different crystal structures (e.g., monoclinic Cu_2S to cubic PbS),[40] or that even structures sharing the same anion sublattice (e.g., PbX to CdX)[37,41] have shown distortions, our results on shape-controlled nanocrystals may therefore aid in a better understanding of cation exchange mechanism in other materials systems.

To ensure maximal removal of the Cu atoms while maintaining the nanodisk shape, we determined the optimal temperature for the cation exchange reaction to be around 180 °C. Under this condition, we synthesized a series of CdTe disks with a red emission that could be tuned continuously from 600 to 640 nm. Figure 6a shows a typical absorption and emission

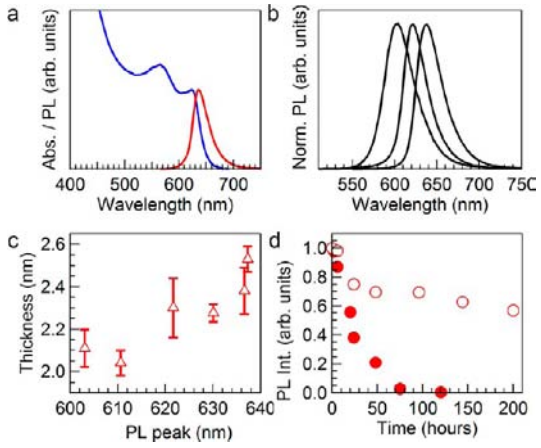

Figure 6. (a) Typical absorbance and PL spectrum, for 10 nm by 2.9 nm CdTe quantum disks. (b) Series of PL spectra. (c) The PL peak position scales with the quantum disk thickness. The error on the average thickness is given as the 95% confidence interval, equal to $1.96\sigma/N^{1/2}$, with σ being the standard deviation and N the number of particles. (d) Optical stability under ambient conditions of CdTe quantum disks compared to spherical CdTe quantum dots obtained by a conventional approach. The PL intensity decreases more slowly with time for the disks.

spectrum, for 10 nm by 2.9 nm CdTe quantum disks, with a series of PL spectra displayed in Figure 6b. PL spectra are typically slightly broader (e.g., 35 nm full width at half-maximum, fwhm, in Figure 6a) than those obtained for spherical CdTe quantum dots (Supporting Information, figure S8), with a small tail toward red wavelengths. This is most likely due to the small thickness and the concurring enhanced sensitivity to size dispersion originating from the strong quantum confinement in this direction. Indeed, a PL excitation spectrum confirms that the typical homogeneous line width at room temperature equals 22 nm (fwhm, for a sample emitting at 637 nm), leading to a substantially narrower peak than the 32 nm ensemble-broadened band-edge absorption (Supporting Information, Figure S9).

Figure 6c shows that the PL peak position is correlated with the quantum disk thickness (see also Supporting Information, Table S2). Note that we used the thickness of the corresponding Cu_2Te nanodisks to plot the data, as the CdTe typically lie flat on the TEM grid, while the Cu_2Te disks easily form aligned stacks allowing an accurate thickness determination (see Figure 1 and Supporting Information, Figure S1). Furthermore, the average, size-independent increase of about 12% (cfr. above) is not expected to affect the overall trend observed in Figure 6c. In contrast, no correlation is observed with the disk diameter (Supporting Information, Figure S10). This does not come unexpected: as the typical diameters are only slightly smaller than the 13.4 nm exciton Bohr diameter in CdTe, confinement effects arising from the small thickness should form the dominant contribution to the PL blue shift.

We measured the PL quantum efficiency (QE) for eight samples, and found an average value of 18.1%, and a peak value of 36% (Table 2). The table also shows that Cu/Cd atomic

Table 2. Cu/Cd Atomic Ratio (determined by ICP-OES), PL Peak Position, and Quantum Efficiency of the Eight Samples Investigated

sample	Cu/Cd ratio (%)	PL (nm)	QE (%)
CdTe_1	0.3	616.4	8.0
CdTe_2	0.09	621.7	14.7
CdTe_3	3	630.0	20.3
CdTe_4	0.03	621.8	31.3
CdTe_5	0.06	636.6	6.0
CdTe_6	2	637.3	36.1
CdTe_7	[a]	603.0	17.2
CdTe_8	[a]	637.7	11.5

[a]For these two samples, the PL QE was measured without determination of the Cu/Cd ratio.

ratios fell well below 1% for all but two samples, supporting the assignment of the PL to band-edge exciton recombination. Comparing the different QE values, no quenching of the band-edge PL with increasing Cu concentration is observed over the different samples, however, it is known that in Cu-doped Zn and Cd chalcogenides, the quenching is weakest in CdTe, possibly due to the energetic position of the Cu-level, only 0.15 eV above the valence band of CdTe (whereas in other materials Cu yields a deep trap state).[42] The quenching might even be further suppressed by a permanent hole present in the Cu-dopant, preventing nonradiative hole relaxation,[43] although this remains to be investigated.

We are not yet at the level of recent results obtained on CdSe core/graded shell quantum dots with efficiencies exceeding 80% in solid state conditions;[44] however, the QE values can still be considered an excellent starting point for further spectroscopic investigations. Moreover, the CdTe quantum disks show an enhanced stability of the PL when stored under ambient conditions compared with their spherical counterparts synthesized by a conventional approach.[45] While the latter quantum dots already lose more than 90% of their initial PL after 60 h, the CdTe quantum disks reported here, despite their larger surface-to-volume ratio, retain 60% of their luminescence even after 10 days (figure 6d). The reason is the efficient passivation of the surface. XPS results collected on the CdTe quantum disks show an S/Te ratio of 0.25/1, in agreement with the parent Cu_2Te nanodisks. However, detailed investigation shows that these S atoms behave differently for Cu_2Te and CdTe when exposed to prolonged X-ray irradiation (Supporting Information, Figure S11). In the case of Cu_2Te, the S 2p peak intensity and hence the sulfur concentration decreased

dx.doi.org/10.1021/ja404694k | J. Am. Chem. Soc. 2013, 135, 12270−12278

with time due to X-ray-induced damage and removal of the thiol capping layer.[46] On the other hand, for CdTe nanodisks the intensity of the S 2p peak remained constant. A deconvolution of the S 2p peak gives more insight into nature of the chemical bonds (Supporting Information, Figure S11c). In the case of the Cu_2Te nanodisks, a good fit was obtained with one doublet, fixing the position of the S $2p_{3/2}$ peak at 162 ± 0.2 eV typical for thiols adsorbed on Cu.[47] On the other hand, in the case of CdTe quantum disks two doublets were needed. In particular, the doublet with higher intensity corresponds to about 89% of the total S content (green curves in panel c), and it is centered at 161.2 ± 0.2 eV, a value typical for CdS.[48] The XPS analysis therefore suggests that, during the cation exchange reaction, the majority of the S atoms in the thiol capping layer bind tightly to the excess Cd on the quantum disk surface, forming an effective monolayer of CdS. This protects the CdTe core from oxidation, leading to the enhanced PL stability.

Finally, the band-edge PL lifetime was measured using time-resolved fluorescence spectroscopy. A typical trace is shown in Figure 7a, for CdTe disks with a 616 nm peak emission. The dominant component of the decay has a lifetime of 9 ns (lifetime-weighted relative amplitude of 65%), yet we used a triexponential decay function in order to adequately fit smaller-weight components with a shorter (1.5 ns, 2%) and longer (23 ns, 33%) lifetime, respectively. Figure 7b shows the spectral dependence of the decay. Averaged over all traces, typical decay times (Figure 7c) and weights corresponded to 3 ± 1.5 ns (5%), 12 ± 2 ns (62%), and 31 ± 7 ns (33%), similar to the decay times at the peak position (Figure 7a). Values increased to 8 ± 2 ns (13%), 20 ± 3 ns (62%), and 59 ± 7 ns (25%), respectively, for CdTe disks with a 637 nm peak emission. Most importantly, in both cases, we did not observe the typical long lifetime of several 100 ns associated with Cu-related emission in metal chalcogenide nanocrystals,[49−52] in agreement with the limited Cu-concentration measured via elemental analysis.

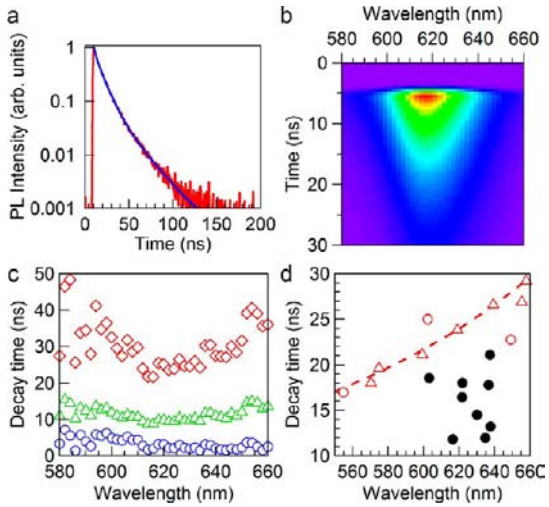

Figure 7. (a) Typical decay trace, for a sample with emission peak at 616 nm, with triexponential fit. (b) Spectral dependence of the decay. (c) Resulting decay components obtained from the fit. (d) Lifetime-weighted average decay time for quantum disks (full dots), spherical quantum dots (open circles), and literature data on dots (triangles). The quantum dot data agree with a fitted curve proposed in ref 47, and the quantum disks show, on average, a 36% faster lifetime.

Figure 7d displays the weighted average decay time for eight CdTe quantum disk samples. Data are consistently smaller than those obtained on spherical quantum dots. The latter fall in the range of 17−25 ns and agree well with literature values,[53] where also a band gap dependence is reported by following equation: $\tau = (-0.0903 + 0.066 \times 1239.85/\lambda_0)^{-1}$,[54] with τ the exciton lifetime and λ_0 the spectral position of the PL peak (Figure 7d, dashed line). The PL lifetime of the disks is more scattered, yielding a band that is approximately 25−45% faster than the spherical quantum dots.

The emission rate τ^{-1} at a given frequency ω is directly proportional to the local field factor $|f_{LF}|^2$ expressing the dielectric screening of the incident and emitted light, and the effective band-edge oscillator strength f_{eff}, taking the exciton distribution over different dark and bright states into account:[55−57]

$$\tau^{-1} = \frac{e^2}{2\pi\varepsilon_0 c^3 m_e} n_S |f_{LF}|^2 \omega^2 f_{eff}, \quad f_{eff} = \frac{\Sigma_k f_k \exp\left(-\frac{\Delta E_k}{kT}\right)}{\Sigma_k g_k \exp\left(-\frac{\Delta E_k}{kT}\right)} \tag{1}$$

where ε_0 equals the dielectric constant, and for each state k, f_k, g_k, and ΔE_k are the oscillator strength, degeneracy, and energetic splitting from the lowest excited state, respectively (g: total band gap degeneracy). A full quantification of the emission rate is beyond the scope of the present paper; however, eq 1 already gives important indications for the faster τ^{-1} in quantum disks. First, the strong confinement of the disks in the lateral dimension allows for a larger nanocrystal volume at a given emission wavelength (see Supporting Information, Figure S10). In line with the increase of the oscillator strength with volume observed for spherical quantum dots,[57,58] at a given emission wavelength, we expect f_{eff} to be larger in the disks leading to a faster τ^{-1}. The peculiar shape will also affect the dielectric screening[55] (see the Supporting Information). We calculated a band-edge $|f_{LF}|^2 = 0.216$ and $|f_{LF}|^2 = 0.308$ for quantum dots and quantum disks, respectively, again favoring a faster emission rate in the quantum disks.

To a certain extent, both may be compensated by the different band-edge states populated at room temperature, as it is known that the shape can also substantially modify the splitting between them.[59,60] Nevertheless, the results point toward a convenient control of the emission lifetime via the shape of the nanocrystals, in this case inducing a faster recombination rate. This is, for instance, beneficial for the design of efficient single (quantum) emitters,[61] as it enhances the single dot brightness.

■ CONCLUSIONS

We have synthesized novel disk-shaped Cu_2Te nanocrystals with a tunable diameter and thickness and a hexagonal crystal structure. Subsequent cation exchange from Cu to Cd at high temperature (180 °C) enabled us to obtain highly fluorescent CdTe nanocrystals, with typically less than 1% of Cu (compared to Cd) remaining in the lattice. While cation exchange reactions maintain the overall shape of the nanocrystal as is also the case here, our data show that they can still imply a substantial restructuring of the anion sublattice. Detailed analysis of the PL lifetime in the resulting CdTe quantum disks allowed us to conclude that it arises from band-edge exciton recombination, and the emission related to Cu-impurity levels was not observed. The PL lifetime was ca. 25−

45% faster than that of spherical quantum dots at the same emission wavelength. Absolute values of the fluorescence quantum efficiency reached up to 36%, with an average of 18% over eight different samples prepared in similar way. Given their peculiar shape as well as the in-plane orientation of the *c*-axis, and taking into account that present quantum efficiencies could still be further enhanced by a development of core/shell nanocrystals, these novel nanostructures may spark a further investigation into the shape and crystal structure dependent optoelectronic band structure of colloidal quantum dots, and find application in future photonic devices such as lasers,[44] LEDs,[62] or quantum emitters.[61]

■ ASSOCIATED CONTENT

Supporting Information

Synthesis protocols to obtain differently sized quantum disks, large-scale TEM image of self-assembled Cu_2Te nanodisks, and additional optical, electron microscopy, X-ray diffraction, and XPS data. This material is available free of charge via the Internet at http://pubs.acs.org.

■ AUTHOR INFORMATION

Corresponding Author

iwan.moreels@iit.it

Author Contributions

H.L. and R.B. contributed equally to the manuscript. The manuscript was written through contributions of all authors.

Notes

The authors declare no competing financial interest.

■ ACKNOWLEDGMENTS

F. De Donato, G. Pugliese, and S. Nitti are acknowledged for collecting the ICP-OES data. The research leading to these results has received funding from the European Union's Seventh Framework Program (FP7/2007-2013) under REA grant agreement no. PIEF-GA-2011-298022 (NIRPLANA) and 240111 (ERC starting grant NANO-ARCH).

■ REFERENCES

(1) Alivisatos, A. P. *Science* **1996**, *271*, 933−937.
(2) Peng, X.; Schlamp, M. C.; Kadavanich, A. V.; Alivisatos, A. P. *J. Am. Chem. Soc.* **1997**, *119*, 7019−7029.
(3) Peng, X. G.; Manna, L.; Yang, W. D.; Wickham, J.; Scher, E.; Kadavanich, A.; Alivisatos, A. P. *Nature* **2000**, *404*, 59−61.
(4) Dong, A.; Tang, R.; Buhro, W. E. *J. Am. Chem. Soc.* **2007**, *129*, 12254−12262.
(5) Carbone, L.; Nobile, C.; De Giorgi, M.; Sala, F. D.; Morello, G.; Pompa, P.; Hytch, M.; Snoeck, E.; Fiore, A.; Franchini, I. R.; Nadasan, M.; Silvestre, A. F.; Chiodo, L.; Kudera, S.; Cingolani, R.; Krahne, R.; Manna, L. *Nano Lett.* **2007**, *7*, 2942−2950.
(6) Ithurria, S.; Tessier, M. D.; Mahler, B.; Lobo, R. P. S. M.; Dubertret, B.; Efros, A. L. *Nat. Mater.* **2011**, *10*, 936−941.
(7) Bouet, C.; Tessier, M. D.; Ithurria, S.; Mahler, B.; Nadal, B.; Dubertret, B. *Chem. Mater.* **2013**, 1262−1271.
(8) Cassette, E.; Mahler, B.; Guigner, J. M.; Patriarche, G.; Dubertret, B.; Pons, T. *ACS Nano* **2012**, *6*, 6741−6750.
(9) Ithurria, S.; Talapin, D. V. *J. Am. Chem. Soc.* **2012**, *134*, 18585−18590.
(10) Sigman, M. B.; Ghezelbash, A.; Hanrath, T.; Saunders, A. E.; Lee, F.; Korgel, B. A. *J. Am. Chem. Soc.* **2003**, *125*, 16050−16057.
(11) Choi, J.; Kang, N.; Yang, H. Y.; Kim, H. J.; Son, S. U. *Chem. Mater.* **2010**, *22*, 3586−3588.
(12) Du, Y.; Yin, Z.; Zhu, J.; Huang, X.; Wu, X.-J.; Zeng, Z.; Yan, Q.; Zhang, H. *Nat. Commun.* **2012**, *3*, 1177.
(13) Li, Z.; Peng, X. *J. Am. Chem. Soc.* **2011**, *133*, 6578−6586.
(14) Hu, S.; Wang, X. *Chem. Soc. Rev.* **2013**, *42*, 5577−5594.
(15) Schliehe, C.; Juarez, B. H.; Pelletier, M.; Jander, S.; Greshnykh, D.; Nagel, M.; Meyer, A.; Foerster, S.; Kornowski, A.; Klinke, C.; Weller, H. *Science* **2010**, *329*, 550−553.
(16) Saunders, A. E.; Ghezelbash, A.; Smilgies, D.-M.; Sigman, M. B.; Korgel, B. A. *Nano Lett.* **2007**, *7*, 541−541.
(17) Ithurria, S.; Dubertret, B. *J. Am. Chem. Soc.* **2008**, *130*, 16504−16505.
(18) Son, D. H.; Hughes, S. M.; Yin, Y. D.; Alivisatos, A. P. *Science* **2004**, *306*, 1009−1012.
(19) Beberwyck, B. J.; Alivisatos, A. P. *J. Am. Chem. Soc.* **2012**, *134*, 19977−19980.
(20) Deka, S.; Miszta, K.; Dorfs, D.; Genovese, A.; Bertoni, G.; Manna, L. *Nano Lett.* **2010**, *10*, 3770−3776.
(21) Jain, P. K.; Amirav, L.; Aloni, S.; Alivisatos, A. P. *J. Am. Chem. Soc.* **2010**, *132*, 9997−9999.
(22) Sadtler, B.; Demchenko, D. O.; Zheng, H.; Hughes, S. M.; Merkle, M. G.; Dahmen, U.; Wang, L.-W.; Alivisatos, A. P. *J. Am. Chem. Soc.* **2009**, *131*, 5285−5293.
(23) Hsu, S.-W.; Bryks, W.; Tao, A. R. *Chem. Mater.* **2012**, *24*, 3765−3771.
(24) Kriegel, I.; Jiang, C.; Rodríguez-Fernández, J.; Schaller, R. D.; Talapin, D. V.; da Como, E.; Feldmann, J. *J. Am. Chem. Soc.* **2011**, *134*, 1583−1590.
(25) Kriegel, I.; Rodríguez-Fernández, J.; Wisnet, A.; Zhang, H.; Waurisch, C.; Eychmuller, A.; Dubavik, A.; Govorov, A. O.; Feldmann, J. *ACS Nano* **2013**, *7*, 4367−4377.
(26) Li, W.; Zamani, R.; Rivera_Gil, P.; Pelaz, B.; Ibáñez, M.; Cadavid, D.; Shavel, A.; Alvarez-Puebla, R. A.; Parak, W. J.; Arbiol, J.; Cabot, A. *J. Am. Chem. Soc.* **2013**, *135*, 7098−7101.
(27) Dilena, E.; Dorfs, D.; George, C.; Miszta, K.; Povia, M.; Genovese, A.; Casu, A.; Prato, M.; Manna, L. *J. Mater. Chem.* **2012**, *22*, 13023−13031.
(28) Li, H.; Brescia, R.; Krahne, R.; Bertoni, G.; Alcocer, M. J. P.; D'Andrea, C.; Scotognella, F.; Tassone, F.; Zanella, M.; De Giorgi, M.; Manna, L. *ACS Nano* **2012**, *6*, 1637−1647.
(29) Bertoni, G.; Grillo, V.; Brescia, R.; Ke, X.; Bals, S.; Catellani, A.; Li, H.; Manna, L. *ACS Nano* **2012**, *6*, 6453−6461.
(30) Miszta, K.; de Graaf, J.; Bertoni, G.; Dorfs, D.; Brescia, R.; Marras, S.; Ceseracciu, L.; Cingolani, R.; van Roij, R.; Dijkstra, M.; Manna, L. *Nat. Mater.* **2011**, *10*, 872−876.
(31) Moulder, J. F.; Stickle, W. F.; Sobol, P. E.; Bomben, K. D. *Handbook of X-ray Photoelectron Spectroscopy*; Perkin-Elmer Corp.: Eden Prairie, MN, 1992.
(32) Carmona-Rodriguez, J.; Lozada-Morales, R.; del Angel-Vicente, P.; Jimenez-Sandoval, O.; Lopez-Calzada, G.; Dahlberg, D.; Jimenez-Sandoval, S. *J. Mater. Chem.* **2011**, *21*, 13001−13008.
(33) Choi, S. H.; An, K.; Kim, E. G.; Yu, J. H.; Kim, J. H.; Hyeon, T. *Adv. Funct. Mater.* **2009**, *19*, 1645−1649.
(34) Li, H.; Zanella, M.; Genovese, A.; Povia, M.; Falqui, A.; Giannini, C.; Manna, L. *Nano Lett.* **2011**, *11*, 4964−4970.
(35) Rivest, J. B.; Jain, P. K. *Chem. Soc. Rev.* **2013**, *42*, 89−96.
(36) Justo, Y. Ph.D. Thesis, Ghent University, 2012, 9789461970893.
(37) Lambert, K.; Geyter, B. D.; Moreels, I.; Hens, Z. *Chem. Mater.* **2009**, *21*, 778−780.
(38) Manna, L.; Wang; Cingolani, R.; Alivisatos, A. P. *J. Phys. Chem. B* **2005**, *109*, 6183−6192.
(39) Rempel, J. Y.; Trout, B. L.; Bawendi, M. G.; Jensen, K. F. *J. Phys. Chem. B* **2006**, *110*, 18007−18016.
(40) Luther, J. M.; Zheng, H.; Sadtler, B.; Alivisatos, A. P. *J. Am. Chem. Soc.* **2009**, *131*, 16851−16857.
(41) Casavola, M.; van Huis, M. A.; Bals, S.; Lambert, K.; Hens, Z.; Vanmaekelbergh, D. *Chem. Mater.* **2011**, *24*, 294−302.
(42) Grandhi, G. K.; Tomar, R.; Viswanatha, R. *ACS Nano* **2012**, *6*, 9751−9763.
(43) Viswanatha, R.; Brovelli, S.; Pandey, A.; Crooker, S. A.; Klimov, V. I. *Nano Lett.* **2011**, *11*, 4753−4758.

(44) Dang, C.; Lee, J.; Breen, C.; Steckel, J. S.; Coe-Sullivan, S.; Nurmikko, A. *Nat. Nanotechnol.* **2012**, *7*, 335−339.
(45) Fiore, A.; Mastria, R.; Lupo, M. G.; Lanzani, G.; Giannini, C.; Carlino, E.; Morello, G.; De Giorgi, M.; Li, Y.; Cingolani, R.; Manna, L. *J. Am. Chem. Soc.* **2009**, *131*, 2274−2282.
(46) Gonella, G.; Terreni, S.; Cvetko, D.; Cossaro, A.; Mattera, L.; Cavalleri, O.; Rolandi, R.; Morgante, A.; Floreano, L.; Canepa, M. *J. Phys. Chem. B* **2005**, *109*, 18003−18009.
(47) Zhang, W. W.; Lu, C. S.; Zou, Y.; Xie, J. L.; Ren, X. M.; Zhu, H. Z.; Meng, Q. J. *J. Colloid Interface Sci.* **2002**, *249*, 301−306.
(48) Naumkin, A. V.; Kraut-Vass, A.; Gaarenstroom, S. W.; Powell, C. J. *NIST X-ray Photoelectron Spectroscopy Database*, http://srdata.nist.gov/xps/.
(49) Jana, S.; Srivastava, B. B.; Acharya, S.; Santra, P. K.; Jana, N. R.; Sarma, D. D.; Pradhan, N. *Chem. Commun.* **2010**, *46*, 2853−2855.
(50) Srivastava, B. B.; Jana, S.; Pradhan, N. *J. Am. Chem. Soc.* **2010**, *133*, 1007−1015.
(51) Gul, S.; Cooper, J. K.; Corrado, C.; Vollbrecht, B.; Bridges, F.; Guo, J.; Zhang, J. Z. *J. Phys. Chem. C* **2011**, *115*, 20864−20875.
(52) Brovelli, S.; Galland, C.; Viswanatha, R.; Klimov, V. I. *Nano Lett.* **2012**, *12*, 4372−4379.
(53) van Driel, A. F.; Allan, G.; Delerue, C.; Lodahl, P.; Vos, W. L.; Vanmaekelbergh, D. *Phys. Rev. Lett.* **2005**, *95*, 6804−6807.
(54) de Mello Donegá, C.; Koole, R. *J. Phys. Chem. C* **2009**, *113*, 6511−6520.
(55) Hens, Z.; Moreels, I. *J. Mater. Chem.* **2012**, *22*, 10406−10415.
(56) Merzbacher, E. *Quantum Mechanics*, 2nd ed; Wiley International: New York, 1970.
(57) Moreels, I.; Lambert, K.; Smeets, D.; De Muynck, D.; Nollet, T.; Martins, J. C.; Vanhaecke, F.; Vantomme, A.; Delerue, C.; Allan, G.; Hens, Z. *ACS Nano* **2009**, *3*, 3023−3030.
(58) Capek, R. K.; Moreels, I.; Lambert, K.; De Muynck, D.; Zhao, Q.; Van Tomme, A.; Vanhaecke, F.; Hens, Z. *J. Phys. Chem. C* **2010**, *114*, 6371−6376.
(59) Empedocles, S. A.; Norris, D. J.; Bawendi, M. G. *Phys. Rev. Lett.* **1996**, *77*, 3873−3876.
(60) Moreels, I.; Rainò, G.; Gomes, R.; Hens, Z.; Stöferle, T.; Mahrt, R. F. *ACS Nano* **2011**, *5*, 8033−8039.
(61) Choy, J. T.; Hausmann, B. J. M.; Babinec, T. M.; Bulu, I.; Khan, M.; Maletinsky, P.; Yacoby, A.; Loncar, M. *Nat. Photonics* **2011**, *5*, 738−743.
(62) Shirasaki, Y.; Supran, G. J.; Bawendi, M. G.; Bulovic, V. *Nat. Photonics* **2013**, *7*, 13−23.